

# Equation of State of CO<sub>2</sub> Shock Compressed to 1 TPa

L. E. Crandall,<sup>1,2</sup> J. R. Rygg,<sup>1,2,3</sup> D. K. Spaulding,<sup>4</sup> T. R. Boehly,<sup>1</sup> S. Brygoo,<sup>5</sup> P. M. Celliers,<sup>6</sup> J. H. Eggert,<sup>6</sup> D. E. Fratanduono,<sup>6</sup> B. J. Henderson,<sup>1,2</sup> M. F. Huff,<sup>1,2</sup> R. Jeanloz,<sup>7</sup> A. Lazicki,<sup>6</sup> P. Loubeyre,<sup>5</sup> M. C. Marshall,<sup>6</sup> D. N. Polsin,<sup>1</sup> M. Zaghoo,<sup>1</sup> M. Millot,<sup>6</sup> and G. W. Collins<sup>1,2,3</sup>

<sup>1</sup>Laboratory for Laser Energetics, Rochester, NY

<sup>2</sup>University of Rochester, Department of Physics

<sup>3</sup>University of Rochester, Department of Mechanical Engineering

<sup>4</sup>University of California, Davis, CA

<sup>5</sup>CEA, France

<sup>6</sup>Lawrence Livermore National Laboratory, Livermore, CA

<sup>7</sup>University of California, Berkeley, CA

(Dated: August 19, 2020)

Equation-of-state (pressure, density, temperature, internal energy) and reflectivity measurements of shock-compressed CO<sub>2</sub> at and above the insulating-to-conducting transition reveal new insight into the chemistry of simple molecular systems in the warm-dense-matter regime. CO<sub>2</sub> samples were precompressed in diamond-anvil cells to tune the initial densities from 1.35 g/cm<sup>3</sup> (liquid) to 1.74 g/cm<sup>3</sup> (solid) at room temperature and were then shock compressed up to 1 TPa and 93,000 K. Variation in initial density enabled us to infer thermodynamic derivatives including specific heat and Gruneisen coefficient, which reveal a complex bonded and moderately ionized state even at the most extreme conditions studied.

At terapascal pressures (10M atm), forces on atoms and molecules are comparable to their intrinsic quantum forces. Carbon dioxide is a simple molecular species with strong and stable chemical bonds at ambient conditions that exhibits complex phase transition behavior under increasing pressure and temperature. The physical, chemical, and thermodynamic behaviors of simple molecules comprising H, C, O, and N at hundreds of GPa and thousands of kelvin are vital to unraveling the dynamo, convective flow, and evolution of giant planets [1–3]. Additionally, CO<sub>2</sub> is an important by-product of reacted chemical explosives and its polarity, conductivity, and diffusivity at high pressure dictate the reactive dynamics of these explosives [4, 5]. The phase diagram of solid carbon dioxide has been extensively studied with heated diamond-anvil cells (DAC's) to 120 GPa [6–11]. This work demonstrates that the warm-dense-fluid regime of CO<sub>2</sub> is equally complex up to TPa pressures.

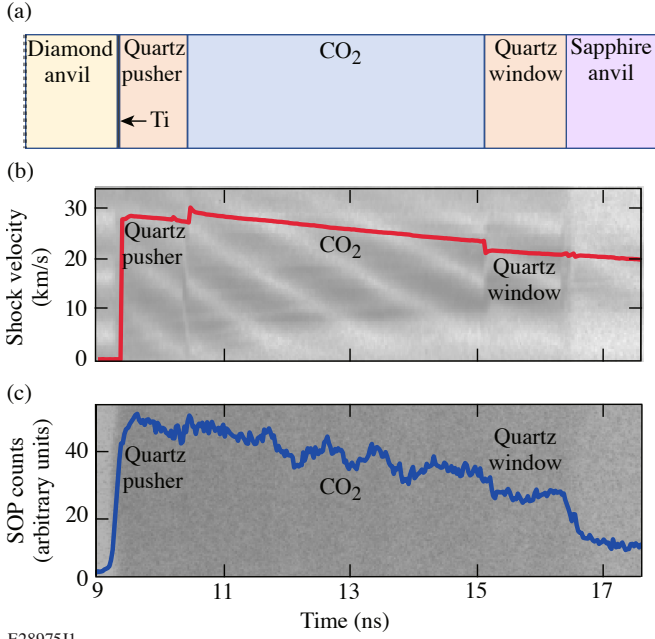
Previous shock-wave data on initially liquid CO<sub>2</sub> ( $\rho_0 = 1.17$  g/cm<sup>3</sup>) up to 71 GPa [12, 13] reveal a deflection in the Hugoniot (locus of material states attainable with a single shock wave) above 30 GPa, which is thought to indicate the onset of molecular dissociation or polymerization. Shock-wave data on initially solid CO<sub>2</sub> ( $\rho_0 = 1.45$  g/cm<sup>3</sup>) [14, 15] extend to 63 GPa and do not exhibit molecular bonding changes. More recently, dynamic compression experiments at the Sandia Z Facility measured the Hugoniot of liquid CO<sub>2</sub> ( $\rho_0 = 1.17$  g/cm<sup>3</sup>) to 840 GPa [16], which was found to compare well with *ab initio* calculations. These experiments measured the mechanical response of CO<sub>2</sub>, and relied on theory to infer thermodynamic behavior. We present the first temperature and reflectivity measurements of shocked CO<sub>2</sub>.

This work uses precompression and laser-driven shocks to explore the CO<sub>2</sub> equation-of-state (EOS) over a wide

range of pressures and temperatures, extending to 1 TPa (10 Mbar) and 93,000 K (8 eV). CO<sub>2</sub> was precompressed to pressures up to 1.16 GPa in DAC's, attaining both liquid and solid initial states, and was then shock compressed. The temperature–pressure–density–internal energy (T, P,  $\rho$ , E) EOS and optical reflectance (R) at 532 nm for these shocks were obtained with a velocity interferometer and an optical pyrometer. These data map a broad range of states from which thermodynamic derivatives were inferred, including the specific heat ( $c_v$ ) and the Gruneisen coefficient ( $\gamma$ ).

Combining these new data with previous results and theoretical calculations [17] reveals a rich and complex phase diagram for CO<sub>2</sub>. The shocked fluid exhibits at least three linear slopes in the shock velocity versus particle velocity plane; this may indicate three distinct phases, or two phases with a transition region. Optical reflectivity measurements reveal an insulator-to-conductor transition between 100 and 200 GPa with a carrier density of roughly 0.3 e<sup>−</sup>/atom. The observed trend in specific heat suggests a complex bonded fluid with increasing molecular degrees of freedom up to 1 TPa, as opposed to an atomic fluid. We find that state-of-the-art modeling needs refinement to match the observed reflectivity and compressibility behavior of CO<sub>2</sub>. High-pressure chemistry was once believed to be rather simple; this work reveals multiform behavior that is potentially quite general, as most of the known matter of the universe exists at high energy density ( $P > 100$  GPa).

These shocked CO<sub>2</sub> experiments were performed at the OMEGA Laser Facility at the Laboratory for Laser Energetics at the University of Rochester [18]. CO<sub>2</sub> samples were precompressed to various initial pressures [19] using DAC's [20, 21] to explore a family of Hugoniots. A schematic of the cell is shown in Fig. 1(a). CO<sub>2</sub> was



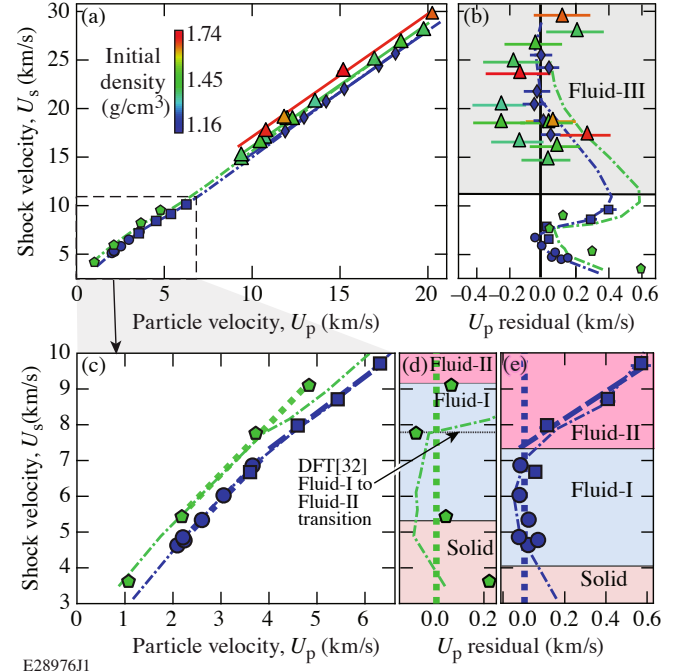
E28975J1

FIG. 1: (a) A schematic of the target stack: CO<sub>2</sub>, sandwiched between quartz references, is precompressed in diamond-sapphire anvil cells to a liquid or solid-I phase before being dynamically compressed with laser-driven shock waves. (b/c) Raw VISAR/SOP streaked images from shot 58922. Overplotted are shock velocity (red) and raw SOP count (blue) temporal profiles. VISAR: velocity interferometer system for any reflector; SOP: streaked optical pyrometer.

cryogenically loaded into cells comprising diamond and sapphire anvils before being mechanically precompressed to initial densities ranging from 1.35 g/cm<sup>3</sup> (liquid [22]) to 1.74 g/cm<sup>3</sup> (solid-I [10]). A gold x-ray shield and a CH plastic ablator (not shown in the schematic) were deposited onto the diamond. Two  $\alpha$ -quartz references were inserted on either side of the CO<sub>2</sub> sample. The OMEGA laser irradiated the diamond side of the DAC with intensities up to  $8 \times 10^{14}$  W/cm<sup>2</sup> to drive shock waves with up to TPa pressures into the precompressed CO<sub>2</sub>.

The velocity of the reflecting shock wave was measured throughout the shock transit of the entire experiment with a dual-channel velocity interferometer system for any reflector (VISAR) [23]. The quartz pusher was used as a reference [24–26] for impedance matching [27] at the pusher/CO<sub>2</sub> interface to determine the pressure and particle velocity of shocked CO<sub>2</sub>. In one shot, a fused-silica pusher served as the reference [28–31]. Density and internal energy were then determined from the Rankine–Hugoniot conservation relations. Uncertainty in the particle velocity, pressure, density, and internal energy were propagated from random experimental uncertainties and systematic uncertainties from the quartz reference with a 100,000 trial Monte Carlo method.

Shock velocity ( $U_s$ ) versus particle velocity ( $U_p$ ) from this work and Refs. [12–16] is plotted in Fig. 2(a). Carbon dioxide is predicted to have at least three phases



E28976J1

FIG. 2: (a) Shock velocity versus particle velocity. Initial density for all data and fits is given by the color bar. Triangles are these OMEGA data; diamonds are Sandia Z data [16]. Solid lines are the fit to the OMEGA and Z data. Dotted-dashed lines are density functional theory (DFT) calculations [32]. Additionally plotted are lower-pressure shock data (circles [12]; squares [13]; pentagons [14]). (b) Residual of data and DFT to the fit to the OMEGA and Z data. (c) Blowup of the low-pressure region. Dotted green and blue lines are linear fits to the Fluid-I data with a single slope. The dashed blue line is a linear fit to Fluid-II data. Coefficients and covariance matrix elements for these fits are given in the Supplemental Materials. (d) Residual of the data from Ref. [14] and the fit to the Fluid-I data for  $\rho_0 = 1.45$  g/cm<sup>3</sup>. (e) Residual of the data from Refs. [12, 13] and the fit to the Fluid-I data for  $\rho_0 = 1.17$  g/cm<sup>3</sup>. Phases are described in the text.

in the shocked fluid regime [17]. The low-pressure [ $U_s < 10$  km/s, blown up in Fig. 2(c)] shock-wave data [12–15] cover three phases. The lowest-pressure datum [14] at 5 GPa is likely solid; this is supported by calculated Hugoniot [32] and the measured melt line of CO<sub>2</sub> [9]. The  $\rho_0 = 1.17$  g/cm<sup>3</sup> data (blue) [12, 13] below  $U_s = 7$  km/s and the  $\rho_0 = 1.45$  g/cm<sup>3</sup> data (green) [14, 15] below 10 km/s exhibit the same linear  $U_s - U_p$  slope (dotted blue and dotted green), which suggests that they are in the same phase, denoted Fluid-I. The residuals of the low-pressure data to the Fluid-I fit are plotted in Figs. 2(d) ( $\rho_0 = 1.45$  g/cm<sup>3</sup>) and 2(e) ( $\rho_0 = 1.17$  g/cm<sup>3</sup>). The 1.17 g/cm<sup>3</sup> data undergo a clear decrease in slope above  $U_s = 7$  km/s [13], as shown in the residual plot in Fig. 2(e) (dashed blue). This trend was a benchmark for density functional theory (DFT) [32] and may be attributed to a change from a molecular fluid to an insulating polymeric fluid [17]. We denote this regime

as Fluid-II. Conversely, no such change in slope is observed in the 1.45 g/cm<sup>3</sup> data, indicating the threshold for the transition must be above 9.65 km/s for this initial density.

The high-pressure ( $U_s > 15$  km/s) shock-wave data exhibit yet another  $U_s - U_p$  slope, implying that another transition(s) must occur below 15 km/s (189 GPa). That transition must produce both a shift and change in slope (or multiple slope changes) as predicted by DFT [32] (dotted-dashed lines), suggesting complex behavior relating to high-pressure chemistry. We performed a linear fit to all existing data between 189 and 995 GPa (these OMEGA data and data from Ref. [16]), including a linear term to account for the initial density of each point:

$$U_s(U_p, \rho_0) = c_0 + sU_p + a\rho_0 \quad (1)$$

Coefficients and covariance matrix elements for this fit are presented in the Supplementary Materials. The high-pressure ( $U_s > 15$  km/s) data fall within two standard deviations of the fit, or a residual 0.32 km/s as shown in Fig. 2(b). We denote this regime as Fluid-III. We cannot rule out that other transitions may exist between  $U_s = 9.65$  and 14.72 km/s, since there are currently no data to constrain this region.

The impedance matching results are shown in pressure-versus-compression ( $\rho/\rho_0$ ) space in Fig. 3. As initial density increases, the CO<sub>2</sub> Hugoniot becomes stiffer. DFT calculations (dotted-dashed lines) [32] agree well with the  $\rho_0 = 1.17$  g/cm<sup>3</sup> data (blue), but the higher-initial-density CO<sub>2</sub> data (green) exhibit less compressibility than that model [32] predicts between 50 and 500 GPa. More-recent LEOS (Livermore equation of state) fits [33] (dashed) match the OMEGA  $\rho_0 = 1.4$  g/cm<sup>3</sup> and 1.7 g/cm<sup>3</sup> data (green and red triangles), but they do not predict the increase in compressibility seen by Nellis *et al.* [13] (blue squares) above 30 GPa.

The self-emission (590 to 850 nm) from the shock was measured using streaked optical pyrometry (SOP) [34]. The brightness temperature was determined from the self-emission and reflectance of the CO<sub>2</sub> shocks, which were referenced to those in quartz [26, 35]. Figure 4(a) shows the average temperature for initially 1.4 g/cm<sup>3</sup> CO<sub>2</sub> (solid green) and 1.7 g/cm<sup>3</sup> CO<sub>2</sub> (solid red); the uncertainty in both temperature and reflectivity was defined as the standard deviation in individual shock velocity bins (75 total bins). Data and total uncertainty for the temperature and reflectivity of individual shots is presented in the Supplemental Materials.

The shock reflectivity at 532 nm, deduced from the VISAR amplitude and intensity as referenced to the known reflectivity of the quartz standard [26, 35], is inset in Fig. 4(a). The reflectivity rises steeply from a few percent at 100 GPa to saturation at 32% above 200 GPa, lower than the theory-predicted saturation of 40% [32] (open black circles). The steep rise is a result of

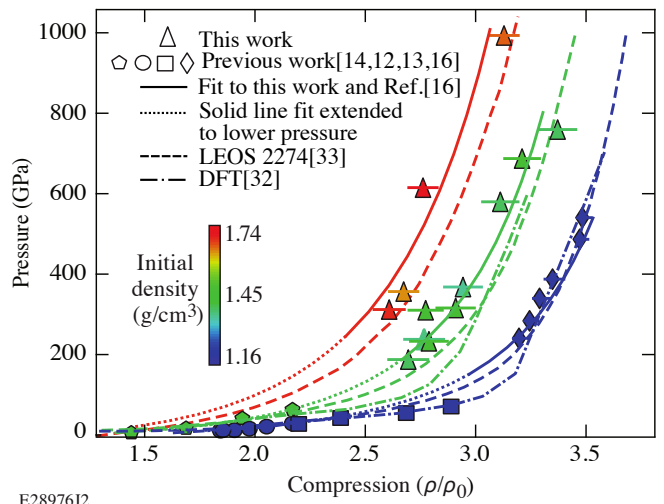


FIG. 3: Pressure versus compression ( $\rho/\rho_0$ ) for shocked CO<sub>2</sub>. Triangles are these OMEGA data; diamonds are Sandia Z data [16]. Additionally plotted are lower-pressure shock data (circles [12]; squares [13]; pentagons [14]). Solid lines are our linear  $U_s(U_p, \rho_0)$  fit given by Eq. (1); dotted lines extend this fit below 189 GPa, the lowest-pressure data point of the fit. Dotted-dashed lines are DFT calculations [32], and dashed lines are LEOS models [33]. Initial density for all data and fits is given by the color bar.

the insulator-to-conductor transition driven by increasing pressure and temperature. Previous theoretical work predicted the onset of metallization to occur as low as 20 GPa [36]. We propose that metallization begins in Fluid-III, above 100 GPa on the Hugoniot. A multiphase fluid regime is constructed in Fig. 4(a) based on trends in the shock velocity of CO<sub>2</sub> in conjunction with theoretical calculations from Ref. [17] that predict a four-fluid system. The predicted boundaries of these fluids were adjusted to be consistent with the observed data.

We infer the dc conductivity plotted in Fig. 4(b) from a Smith-Drude model. This modification to the Drude free-electron model employs a backscattering parameter  $c$  to capture non-Drude-like reductions in electron velocity [38, 39]. The electron density is defined as  $n_e = zn_i$ , and the ionization  $z$  is varied until the model yields the measured reflectivity. Utilizing the Fresnel reflectivity and a minimum scattering time from the Ioffe Regel limit [40–42], the dc conductivity saturates to 2500  $\Omega^{-1}\text{cm}^{-1}$  for minimum backscattering ( $c=0$ ) and the inferred carrier density tends toward 0.3 e-/atom of atomic CO<sub>2</sub>. Ionization tends to unity and dc conductivity saturates to 3500  $\Omega^{-1}\text{cm}^{-1}$  for moderate backscattering of  $c=0.5$ . We assume the scattering to be from fully dissociated CO<sub>2</sub> in the model; if molecular CO<sub>2</sub> was the cause of the scattering, the dc conductivity would decrease by approximately 250  $\Omega^{-1}\text{cm}^{-1}$ . We predict that at a higher temperature, the reflectivity and conductivity would experience another rise as we reach a regime in which additional carriers contribute to the conduction. This behavior will lead to some eventual saturation until

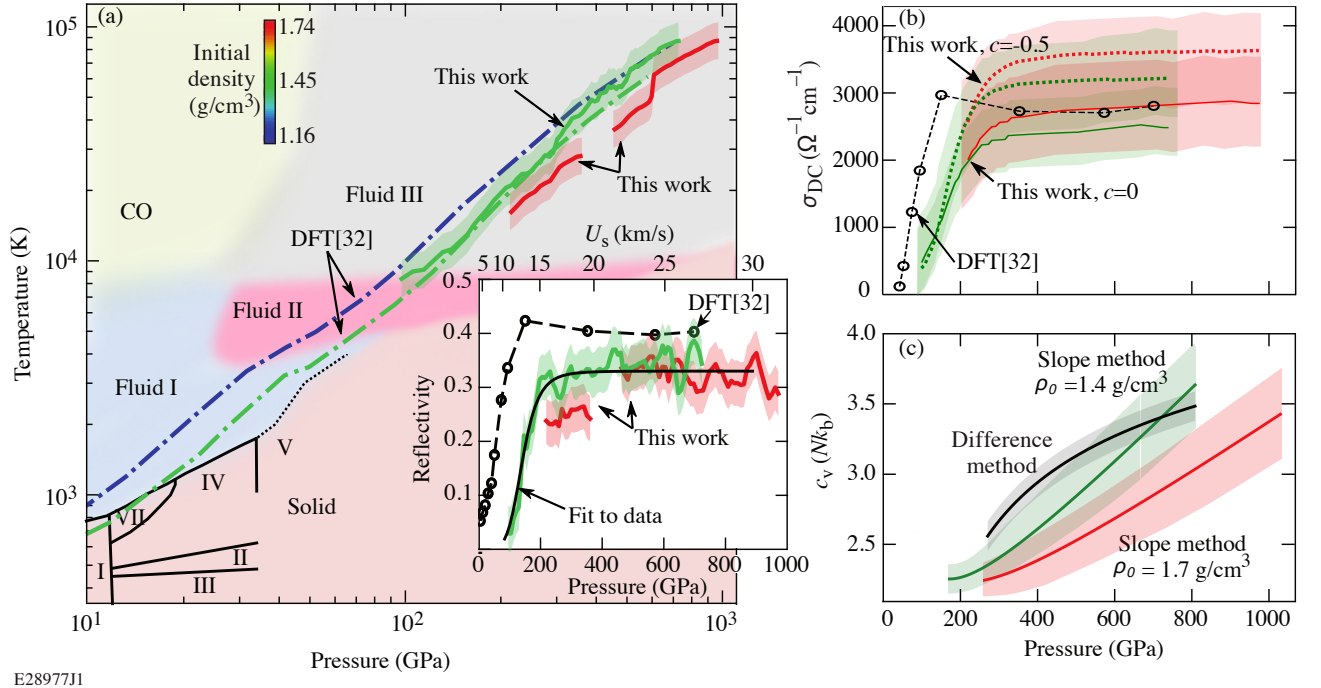


FIG. 4: (a) Red and green solid lines are average decaying-shock temperature versus pressure for these OMEGA CO<sub>2</sub> data; the shading represents random uncertainty and the color represents initial density as given by the color bar. Dotted-dashed lines are DFT calculations [32]. Solid black lines are measured phase boundaries [7, 9], and the dotted black line is a calculated continuation of the melt curve [37]. Shaded regions indicate phases as described in the text. Inset: Average reflectivity at 532 nm versus pressure for the decaying shocks. The shock velocity axis (top) is mapped from the pressure axis (bottom) using Eq. (1) for  $\rho_0 = 1.4$  g/cm<sup>3</sup> and the Rankine-Hugoniot conditions. The solid black line is a Hill fit to all of the reflectivity versus shock velocity data. DFT (open circles connected by a dashed line) [32] predicts a lower-pressure threshold for the insulating-to-conducting transition and higher reflectivity upon saturation. (b) The dc conductivity for these data is inferred from our measured reflectivities by a Smith-Drude model with  $c=0$  (solid) and  $c=-0.5$  (dotted). Additionally plotted is the DFT-predicted conductivity of CO<sub>2</sub> (black open circles) [32]. (c) Green (red) is isochoric specific heat ( $c_v$ ) determined from the slope of the Hugoniot with initial density 1.4 (1.7) g/cm<sup>3</sup>, and black is  $c_v$  as determined from a difference method between the two Hugoniots. Shading represents a  $1\sigma$  confidence interval.

the carriers are no longer degenerate.

The range of initial densities provides Hugoniots for both initially solid and liquid CO<sub>2</sub> and facilitates calculations of thermodynamic derivatives using both a slope method and a difference method at a constant volume [35]. From the mechanical equation of state given by Eq. (1), we calculated the average CO<sub>2</sub> Gruneisen parameter over the pressure range studied to be  $\gamma = V \frac{\partial P}{\partial E}|_V = 0.63 \pm 0.04$ . This value is close to that found both experimentally and theoretically in SiO<sub>2</sub> at 1 TPa [24, 35].

Simultaneous temperature measurements allow one to calculate the isochoric specific heat  $c_v = \frac{\partial E}{\partial T}|_V$ . The slope method [35] allows for calculation of the specific heat along the Hugoniot of initially liquid (green,  $\rho_0 = 1.4$  g/cm<sup>3</sup>) and initially solid (red,  $\rho_0 = 1.7$  g/cm<sup>3</sup>) CO<sub>2</sub>. Uncertainties in thermodynamic derivatives were propagated from the uncertainties in pressure, density, internal energy, and temperature using a 100,000 trial Monte Carlo method. As plotted in Fig. 4(c), the specific heat is steadily increasing from 200 GPa to 1 TPa for both initially liquid and solid CO<sub>2</sub>. The difference method (black), independent from the slope method,

corroborates the trend of increasing specific heat. Increasing specific heat indicates increasing degrees of freedom (DOF's) in the fluid; because reflectivity is constant above 200 GPa, the increasing DOF's is not due to a rising carrier density. We conclude that the electrically conducting Fluid-III phase consists of a moderately ionized and bonded species of increasing chemical complexity, rather than a simple atomic fluid undergoing increasing ionization.

In summary, this work extends pressure and density measurements of the initially liquid and initially solid CO<sub>2</sub> Hugoniot to 1 TPa and provides the first temperature measurements of shocked CO<sub>2</sub> to 93,000 K. We propose a fluid phase diagram comprising at least three regimes to describe all existing shocked CO<sub>2</sub> data. Reflectivity and specific heat trends indicate that at pressures reaching 1 TPa, CO<sub>2</sub> is not likely a simple atomic fluid but instead a complex bonded and partially ionized species. Current models do not predict the observed compressibility and metallization behavior of high-pressure CO<sub>2</sub>. This work demonstrates the rich behavior of nominally simple materials at high energy density and invites

further inquiry into the chemistry of warm dense matter.

### Acknowledgments

This material is based upon work supported by the Department of Energy National Nuclear Security Administration under Award Number DE-NA0003856, the University of Rochester, and the New York State Energy Research and Development Authority. A portion of this work was conducted at Lawrence Livermore National Laboratory under Contract Number DE-AC52-07NA27344.

This report was prepared as an account of work sponsored by an agency of the U.S. Government. Neither the U.S. Government nor any agency thereof, nor any of their employees, makes any warranty, express or implied, or assumes any legal liability or responsibility for the accuracy, completeness, or usefulness of any information, apparatus, product, or process disclosed, or represents that its use would not infringe privately owned rights. Reference herein to any specific commercial product, process, or service by trade name, trademark, manufacturer, or otherwise does not necessarily constitute or imply its endorsement, recommendation, or favoring by the U.S. Government or any agency thereof. The views and opinions of authors expressed herein do not necessarily state or reflect those of the U.S. Government or any agency thereof.

- 
- [1] T. Guillot, *Science* **286**, 72 (1999).
  - [2] C. Cavazzoni, G. L. Chiarotti, S. Scandolo, E. Tosatti, M. Bernasconi, and M. Parrinello, *Science* **283**, 44 (1999).
  - [3] S. Stanley and J. Bloxham, *Nature* **428**, 151 (2004).
  - [4] M. van Thiel and F. H. Ree, *J. Appl. Phys.* **62**, 1761 (1987).
  - [5] V. V. Chaban, E. E. Fileti, and O. V. Prezhdo, *J. Phys. Chem. Lett.* **6**, 913 (2015).
  - [6] K. F. Dziubek, M. Ende, D. Scelta, R. Bini, M. Mezouar, G. Garbarino, and R. Miletich, *Nat. Commun.* **9**, 3148 (2018).
  - [7] F. Datchi and G. Weck, *Z. Kristallogr.* **229**, 135 (2014).
  - [8] C.-S. Yoo, *Phys. Chem. Chem. Phys.* **15**, 7949 (2013).
  - [9] K. D. Litasov, A. F. Goncharov, and R. J. Hemley, *Earth Planet. Sci. Lett.* **309**, 318 (2011).
  - [10] V. M. Giordano, F. Datchi, F. A. Gorelli, and R. Bini, *J. Chem. Phys.* **133**, 144501 (2010).
  - [11] V. M. Giordano, F. Datchi, and A. Dewaele, *J. Chem. Phys.* **125**, 054504 (2006).
  - [12] G. L. Schott, *High Press. Res.* **6**, 187 (1991).
  - [13] W. J. Nellis, A. C. Mitchell, F. H. Ree, M. Ross, N. C. Holmes, R. J. Trainor, and D. J. Erskine, *J. Chem. Phys.* **95**, 5268 (1991).
  - [14] V. N. Zubarev and G. S. Telegin, *Sov. Phys.-Dokl.* **7**, 34 (1962).
  - [15] Zubarev and Telegin [14] report two different initial densities for their solid CO<sub>2</sub>: 1.45 and 1.54 g/cm<sup>3</sup>. Cited in Schott [12] are “verbal inquires and replies conveyed through C. L. Mader and A. N. Dremin, *ca.* 1983” that confirm that 1.54 g/cm<sup>3</sup> is a misprint, and the initial density of the data published by Zubarev and Telegin is 1.45 g/cm<sup>3</sup>.
  - [16] S. Root, K. R. Cochrane, J. H. Carpenter, and T. R. Mattsson, *Phys. Rev. B* **87**, 224102 (2013).
  - [17] B. Boates, A. M. Teweldeberhan, and S. A. Bonev, *Proc. Natl. Acad. Sci.* **109**, 14808 (2012).
  - [18] T. R. Boehly, D. L. Brown, R. S. Craxton, R. L. Keck, J. P. Knauer, J. H. Kelly, T. J. Kessler, S. A. Kumpan, S. J. Loucks, S. A. Letzring *et al.*, *Opt. Commun.* **133**, 495 (1997).
  - [19] G. J. Piermarini, S. Block, J. D. Barnett, and R. A. Forman, *J. Appl. Phys.* **46**, 2774 (1975).
  - [20] J. Eggert, S. Brygoo, P. Loubeyre, R. S. McWilliams, P. M. Celliers, D. G. Hicks, T. R. Boehly, R. Jeanloz, and G. W. Collins, *Phys. Rev. Lett.* **100**, 124503 (2008).
  - [21] P. M. Celliers, P. Loubeyre, J. H. Eggert, S. Brygoo, R. S. McWilliams, D. G. Hicks, T. R. Boehly, R. Jeanloz, and G. W. Collins, *Phys. Rev. Lett.* **104**, 184503 (2010).
  - [22] S. M. Sterner and K. S. Pitzer, *Contrib. Mineral. Petr.* **117**, 362 (1994).
  - [23] P. M. Celliers, D. K. Bradley, G. W. Collins, D. G. Hicks, T. R. Boehly, and W. J. Armstrong, *Rev. Sci. Instrum.* **75**, 4916 (2004).
  - [24] M. D. Knudson and M. P. Desjarlais, *Phys. Rev. B* **88**, 184107 (2013).
  - [25] M. P. Desjarlais, M. D. Knudson, and K. R. Cochrane, *J. Appl. Phys.* **122**, 035903 (2017).
  - [26] S. Brygoo, M. Millot, P. Loubeyre, A. E. Lazicki, S. Hamel, T. Qi, P. M. Celliers, F. Coppari, J. H. Eggert, D. E. Fratanduono *et al.*, *J. Appl. Phys.* **118**, 195901 (2015).
  - [27] Ya. B. Zeldovich and Yu. P. Razer, in *Physics of Shock Waves and High-Temperature Hydrodynamic Phenomena*, edited by W. D. Hayes and R. F. Probstein (Dover Publications, Mineola, NY, 2002).
  - [28] C. A. McCoy, M. C. Gregor, D. N. Polsin, D. E. Fratanduono, P. M. Celliers, T. R. Boehly, and D. D. Meyerhofer, *J. Appl. Phys.* **119**, 215901 (2016).
  - [29] C. Meade and R. Jeanloz, *Phys. Rev. B* **35**, 236 (1987).
  - [30] R. G. Kraus, S. T. Stewart, D. C. Swift, C. A. Bolme, R. F. Smith, S. Hamel, B. D. Hammel, D. K. Spaulding, D. G. Hicks, J. H. Eggert *et al.*, *J. Geophys. Res.* **117**, E09009 (2012).
  - [31] The fused silica isentropic release is discussed in the Supplementary Materials.
  - [32] B. Boates, S. Hamel, E. Schwegler, and S. A. Bonev, *J. Chem. Phys.* **134**, 064504 (2011).
  - [33] C. J. Wu, D. A. Young, P. A. Sterne, and P. C. Myint, *J. Chem. Phys.* **151**, 224505 (2019).
  - [34] J. E. Miller, T. R. Boehly, A. Melchior, D. D. Meyerhofer, P. M. Celliers, J. H. Eggert, D. G. Hicks, C. M. Sorce, J. A. Oertel, and P. M. Emmel, *Rev. Sci. Instrum.* **78**, 034903 (2007).
  - [35] D. G. Hicks, T. R. Boehly, J. H. Eggert, J. E. Miller, P. M. Celliers, and G. W. Collins, *Phys. Rev. Lett.* **97**, 025502 (2006).
  - [36] C. Wang and P. Zhang, *J. Chem. Phys.* **133**, 134503 (2010).
  - [37] A. M. Teweldeberhan, B. Boates, and S. A. Bonev, *Earth Planet. Sci. Lett.* **373**, 228 (2013).
  - [38] N. V. Smith, *Phys. Rev. B* **64**, 155106 (2001).
  - [39] R. S. McWilliams, D. A. Dalton, M. F. Mahmood, and

- A. F. Goncharov, Phys. Rev. Lett. **116**, 255501 (2016).
- [40] P. M. Celliers, G. W. Collins, D. G. Hicks, M. Koenig, E. Henry, A. Benuzzi-Mounaix, D. Batani, D. K. Bradley, L. B. Da Silva, R. J. Wallace *et al.*, Phys. Plasmas **11**, L41 (2004).
- [41] D. G. Hicks, P. M. Celliers, G. W. Collins, J. H. Eggert, and S. J. Moon, Phys. Rev. Lett. **91**, 035502 (2003).
- [42] M. Millot, S. Hamel, J. R. Rygg, P. M. Celliers, G. W. Collins, F. Coppari, D. E. Fratanduono, R. Jeanloz, D. C. Swift, and J. H. Eggert, Nat. Phys. **14**, 297 (2018).